


Spatio-temporal characterization of ultrashort vector pulses

Cite as: APL Photonics **6**, 116103 (2021); <https://doi.org/10.1063/5.0056066>

Submitted: 06 May 2021 • Accepted: 17 October 2021 • Accepted Manuscript Online: 17 October 2021 • Published Online: 08 November 2021

 Apostolos Zdagkas,  Venkatram Nalla,  Nikitas Papasimakis, et al.

COLLECTIONS

 This paper was selected as Featured



View Online



Export Citation



CrossMark

ARTICLES YOU MAY BE INTERESTED IN

Fractal-like photonic lattices and localized states arising from singular and nonsingular flatbands

APL Photonics **6**, 116104 (2021); <https://doi.org/10.1063/5.0068032>

A perspective on twisted light from on-chip devices

APL Photonics **6**, 110901 (2021); <https://doi.org/10.1063/5.0060736>

Trapping light in a Floquet topological photonic insulator by Floquet defect mode resonance

APL Photonics **6**, 116101 (2021); <https://doi.org/10.1063/5.0061950>



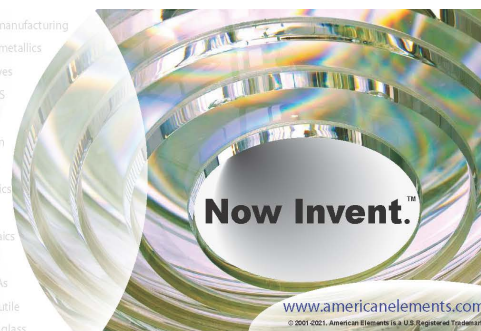
yttrium iron garnet glassy carbon beamsplitters fused quartz additive manufacturing
zeolites III-IV semiconductors gallium lump copper nanoparticles organometallics
nano ribbons barium fluoride europium phosphors photonics infrared dyes

epitaxial crystal growth ultra high purity materials transparent ceramics CIGS
cerium oxide polishing powder MBE grade materials thin film
surface functionalized nanoparticles

sapphire windows Nd:YAG spintronics raman substrates silver nanoparticles perovskites
MOCVD beta-barium borate rare earth metals quantum dots osmium scintillation Ce:YAG
refractory metals laser crystals anode lithium niobate InAs wafers
dysprosium pellets MOFs AuNPs chalcogenides ZnS CdTe perovskite crystals transparent ceramics

metamaterials borosilicate glass YBCO superconductors InGaAs indium tin oxide MgF₂ rutile diamond micropowder optical glass

The Next Generation of Material Science Catalogs



Spatio-temporal characterization of ultrashort vector pulses

Cite as: APL Photon. 6, 116103 (2021); doi: 10.1063/5.0056066

Submitted: 6 May 2021 • Accepted: 17 October 2021 •

Published Online: 8 November 2021



Apostolos Zdagkas,^{1,a)}  Venkatram Nalla,¹  Nikitas Papasimakis,¹  and Nikolay I. Zheludev^{1,2} 

AFFILIATIONS

¹ Optoelectronics Research Centre and Centre for Photonic Metamaterials, University of Southampton, Southampton SO17 1BJ, United Kingdom

² Centre for Disruptive Photonic Technologies, School of Physical and Mathematical Sciences and The Photonics Institute, Nanyang Technological University, Singapore 637378, Singapore

^{a)} Author to whom correspondence should be addressed: A.Zdagkas@soton.ac.uk

ABSTRACT

Ultrafast vectorially polarized pulses have found many applications in information and energy transfer owing mainly to the presence of strong longitudinal components and their space-polarization non-separability. Due to their broad spectra, such pulses often exhibit space-time couplings, which significantly affect the pulse propagation dynamics. Although such couplings usually result in reduced energy density at the focal spot, they have been utilized to demonstrate pulse shaping as in the case of a rotating or sliding wavefront as the pulse travels through its focal point. Here, we present a new method for the spatiotemporal characterization of ultrashort cylindrical vector pulses based on a combination of spatially resolved Fourier transform spectroscopy and Mach-Zehnder interferometry. The method provides access to spatially resolved spectral amplitudes and phases of all polarization components of the pulse. We demonstrate the capabilities of the method by completely characterizing a 10 fs radially polarized pulse from a Ti:sapphire laser centered at 800 nm.

© 2021 Author(s). All article content, except where otherwise noted, is licensed under a Creative Commons Attribution (CC BY) license (<http://creativecommons.org/licenses/by/4.0/>). <https://doi.org/10.1063/5.0056066>

I. INTRODUCTION

Space-time couplings (STCs) in propagating waves are defined as the dependence of the temporal properties of the electric field on the transverse spatial coordinates.¹ Mathematically, they are revealed as the non-separability of the spatial and temporal terms of the electric field of a pulse into a product, $E(\mathbf{r}, t) \neq f(\mathbf{r})g(t)$. They can significantly affect the energy density of ultrashort pulses at focus² since, in most cases, pulses possessing STCs can only be locally transform limited owing to the fact that each position may contain only a subset of the overall spectrum. STCs also alter the propagation dynamics of ultrashort pulses. The latter has been utilized to create new effects like the attosecond lighthouse³ where a tilted wavefront is transformed to a rotating wavefront at focus and the “sliding” or “flying” focus^{4,5} where STCs create a focal spot that locally travels with speed greater or lower than the speed of light in free space.

A range of techniques have been demonstrated for the complete spatiotemporal characterization (retrieval of electric field amplitude

and phase) of linearly polarized pulses.⁶ Such approaches are typically based on scanning the transverse profile of the unknown pulse with a known reference pulse⁷ or utilize concepts from wavefront characterization techniques.⁸ Single shot methods have been developed that can characterize either a spatial slice of the pulse^{9–11} or the whole pulse on a single measurement.¹² Moreover, self-referenced methods have been proposed, where a small part of the pulse under characterization is used as reference. In the latter, the reference is interfered with the unknown pulse and the unknown spectral phase is retrieved through spatially resolved Fourier transform spectroscopy.¹³ A variation of the latter, named TERMITES,¹⁴ uses a slightly expanded replica of the unknown pulse along with an iterative algorithm as a way to reduce the requirements of creating a very homogeneous reference pulse.

However, none of the aforementioned methods has been applied for the simultaneous characterization of the spatially dependent polarization, intensity, and phase that vector polarized pulses exhibit. For example, the TERMITES method does not provide the required polarization information for the characterization of

cylindrical vector pulses (CVPs), such as radially polarized pulses that exhibit polarization singularities at their center, but it can be used as the basis for a method that can. Ultrafast radially polarized pulses have been generated in the femtosecond regime¹⁵ and have been compressed down to few femtoseconds.^{16,17} Due to their broad spectra, such pulses often exhibit space–time couplings (STCs). Moreover, space–time couplings may have been prescribed to them through a metamaterial converter.¹⁸ Since CVPs cover a diverse range of applications (see the Appendix) and space–time couplings can significantly affect their properties, their characterization is important.

The complete characterization of CVPs has been limited mainly to their spatially varying polarization profile. The temporal profile of such pulses has been characterized independently by standard approaches, such as FROG¹⁹ and SPIDER.²⁰ However, such measurements are performed at a single spatial position or a slice^{9–11} of the cross section of the pulse, which is far from a complete characterization of the pulses that may exhibit STCs.¹ For example, theoretical calculations have shown that the flying donut pulse is isodiffracting,²¹ a property that leads to the spatial profiles of intensity for every frequency component of the pulse to scale along the trajectory of the pulse in the same way. Furthermore, since most ultrafast systems use pulse compressors based on prisms or gratings, in order to implement chirped pulse amplification (CPA),²² the appearance of pulse front tilt (PFT) is very likely to occur from small misalignments^{1,2} leading to detrimental effects for the pulse duration and its energy density. The PFT distorts the temporal shape of the pulse. Such space–time couplings occur also in the case of ultrafast CVPs²³ and can lead to dramatic effects on the pulse shape and propagation. For example, Fig. 1 illustrates the effect of pulse front tilt and pulse front curvature on the shape of a radially polarized pulse. PFT appears as a linearly varying delay of the pulse across a transverse direction, while the pulse front curvature is a quadratically varying delay from the center of the pulse to its edges.

Recently, a new method has been utilized for the complete spatiotemporal characterization of a 100 fs vector pulse through a twofold interferometer,²⁴ and it was shown to successfully characterize spatially varying polarization gates. However, it is based on a point by point scan scheme, which may render it impractical for the complete transverse spatial characterization of a pulse when high resolution is required.

In this work, we present a method for the complete spatiotemporal characterization of CVPs based on Fourier transform spectroscopy^{25,26} and, in particular, on TERMITES.¹⁴ The method is an extension of the TERMITES technique by means of a Mach–Zehnder interferometer and is termed TERMITES-MAZE (Mach–Zehnder Extended). The extension renders the method capable of characterizing the spatial and temporal profile of all polarization components of ultrafast CVPs at the spatial resolution of a camera sensor. We illustrate the capabilities of the TERMITES-MAZE technique by applying it to the case of a 10 fs radially polarized pulse centered at 800 nm. We show that our approach can reveal the space–time couplings (e.g., pulse front tilt) across different planes for different polarization components of the pulse. We present a detailed description of the experimental implementation of TERMITES-MAZE, while the corresponding algorithm for the analysis of the experimental data is freely available under the Berkeley Software Distribution (BSD) three-clause license as a Python module.²⁷

As few cycle laser pulses with vectorial fields, orbital angular momentum (OAM),²⁸ and other forms of structured light^{29–31} are increasingly studied, there is a demand for powerful pulse characterization methods. In particular, the presence of STCs becomes increasingly important in such broadband pulses as it can dramatically alter their propagation properties³² and their interaction with matter.^{33,34} The TERMITES-MAZE method introduced here has the capability to characterize all these types of space–time-polarization non-separable light that are increasingly studied³⁵ and thus has the potential to accelerate the research and emerging applications based on few cycle vector structured light.

II. METHOD

A method for the complete characterization of a CVP should provide all the characteristics of the pulse, such as the polarization, spectral amplitude, and spectral phase at each spatial position. The TERMITES-MAZE approach is capable of retrieving all these characteristics, up to a constant phase offset corresponding to the carrier envelope phase that it is not retrieved, through interference of a linearly polarized reference pulse with an unknown CVP. First, the TERMITES method¹⁴ is applied for the characterization of the reference pulse and then a Mach–Zehnder

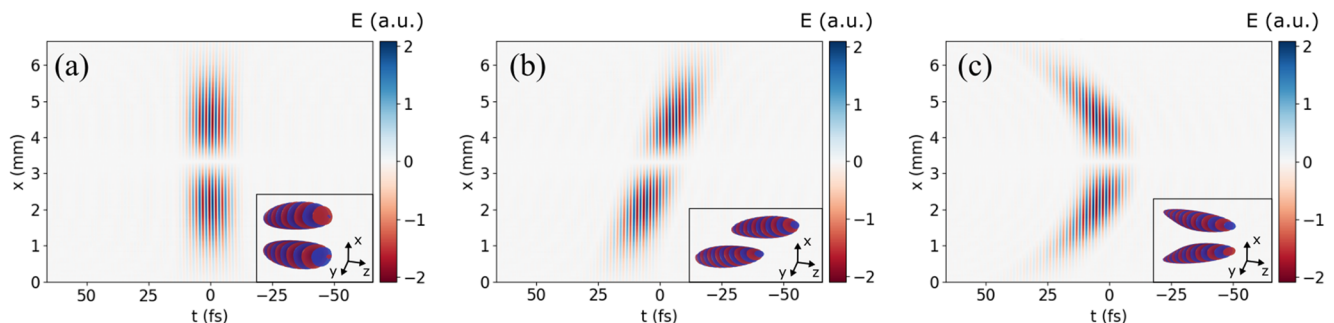


FIG. 1. Characteristic examples of space–time couplings in vector polarized pulses. Cross sections of the x component of the instantaneous electric field of a radially polarized pulse (a) in the absence of space–time couplings, (b) with pulse front tilt (3 fs/mm), and (c) with pulse front curvature (3 fs/mm²). The insets to (a)–(c) present corresponding 3D illustrations in the form of isosurfaces. The pulse propagates along the positive z axis.

interferometer is implemented for the characterization of the unknown pulse. In this way, only one polarization of the CVP is characterized at a time. Finally, since all spatial information is captured, the complete vectorial shape of the pulse can be reconstructed.

A. Experimental implementation

The TERMITES-MAZE method is an extension of the TERMITES method,¹⁴ and as such, it comprises two experiments. In the first experiment a reference linearly polarized pulse is characterized using the TERMITES method, while the second involves a Mach-Zehnder interferometer in which an unknown pulse, in our case a CVP, and the reference pulse are interfered. In both cases, Figs. 2(a) and 2(b), a 10 fs Ti:Sa laser with peak wavelength at 800 nm (Spectra-Physics, Element PRO) is used to generate a linearly polarized pulse. The pulse then travels through a pulse shaper that uses a spatial light modulator (SLM) (Biophotonic solutions, Inc., MIIPS Box640). A polarizer after the pulse shaper is used to remove any unwanted polarization changes introduced by the SLM. The pulse shaper is used to compress the ultrafast pulse to its Fourier limited duration at the plane of detection. Then, a beam expander doubles the beam width in order to fill a segmented waveplate that transforms a linearly polarized beam to a radially polarized one. After the beam expander, a 50:50 beam splitter (BS1 in Fig. 2) is used to generate two replicas of the pulse. Up to this point, the setup is common to both experiments. In the following, we describe the two experiments separately.

The TERMITES experimental setup consists of a Michelson interferometer and a digital camera (Thorlabs DCC1545M); see the upper part of Fig. 2(a) (image sensor). One arm of the interferometer includes a nanometer precision delay line (Thorlabs TSGNF5 single axis piezoelectric stage) with a scanning range of 20 μm . The piezoelectric stage is programmed to move in steps of 20 nm, which correspond to a 40 nm ($\sim\lambda/20$) delay for the pulse. The other arm includes a convex mirror, whose purpose is to expand the unknown

pulse. Hence, the image on the camera sensor will be the result of a pulse interfering with an expanded replica of its central part. This expanding central part is considered more uniform, in terms of spatiotemporal couplings, than the pulse itself since it is just an expanded copy of a small part of the pulse. The TERMITES algorithm requires only knowledge of the expansion factor, and therefore, the central part does not need to be space-time uncoupled. A polarizer is finally placed before the camera to increase the signal to noise ratio.

The TERMITES algorithm reveals the spectral phase differences between every point of the pulse and its center. A temporal characterization of its central part is the only requirement for a complete spatiotemporal characterization. In our case, the “Multiphoton Intrapulse Interference Phase Scan” (MIIPS)³⁶ technique is used for this purpose. More specifically, instead of characterizing the temporal shape of the pulse, we compress it and then a Fourier limited pulse is assumed at the pulse center. The laser pulse is compressed by a commercial pulse shaper (Biophotonic Solutions, MIIPS Box640) producing a 10 fs Fourier transform limited pulse, which is also used for the generation of a Fourier transform limited CVP. The compression process takes less than 10 minutes. The power of the laser varies less than 0.5% over a 20 h period, while the duration of the pulse as characterized by the MIIPS method exhibits fluctuations of 0.1 fs. Each captured image is the result of about 10^6 pulses. Therefore, short term fluctuations are averaged out.

The compression part of the setup can be seen in the lower part of Fig. 2(a). An iris placed before the first beam splitter (BS1) selects only the central part of the pulse for compression that is focused at a second harmonic generation crystal. A filter (F) blocks the fundamental part of the spectrum and transmits only the second harmonic part. The generated spectral intensities are then recorded by a spectrometer (Ocean Optics USB2000 + XR1-ES, 0.5 nm spectral resolution) and fed to the pulse shaper’s software, where the MIIPS

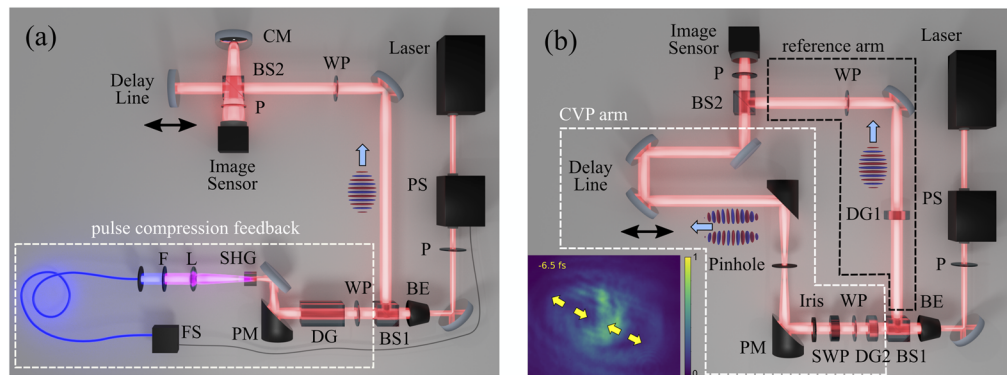


FIG. 2. Experimental implementation of TERMITES-MAZE. The experimental procedure is split into two parts. The first part involves the characterization of a linearly polarized pulse [panel (a)], while the second involves the characterization and retrieval of a CVP [panel (b)]. (a) A Michelson interferometer setup with a convex mirror in one arm and a delay line in the other is used for the spatiotemporal characterization of a linearly polarized pulse (this pulse will be used as reference). The pulse compression part is shown in the lower part of the setup. (b) A Mach-Zehnder interferometer setup with the one arm carrying the reference pulse [as characterized in (a)] and the other hosting the setup for the generation of the CVP. A delay line is used to scan the unknown pulse with the reference. An interference image of the captured intensity at -6.5 fs delay between the linearly polarized pulse and the CVP is shown in the inset. The colorbar corresponds to intensity. The generated images are then used to extract the spectral phase and frequency distribution of the unknown pulse. PS: pulse shaper, P: polarizer, BE: beam expander, BS: beam splitter, WP: $\lambda/2$ waveplate, DG: dispersive glass, PM: parabolic mirror, SHG: second harmonic generation crystal, L: lens, F: filter, FS: fiber spectrometer, CM: convex mirror, and SWP: segmented waveplate.

method is used for the compression. The iris is removed after the pulse compression is completed. In the schematic of Fig. 2(a), the dispersive glass (DG) and the waveplate of the lower arm are used to create the same amount of dispersion as the upper arm. Since the TERMITES setup requires two passes through a beam splitter and one pass through a polarizer, the dispersive glass (DG) in Fig. 2(a) corresponds to two beam splitters and a polarizer. Therefore, the pulse arriving at the camera sensor is still a Fourier transform limited pulse.

A spatial resolution of at least two pixels per fringe period is required to resolve all the fringes and avoid 2π phase jumps across neighboring pixels during the processing of the data. Hence, a careful choice of the convex mirror induced curvature and the camera sensor is necessary. The same is true for the temporal resolution of the delay line. Therefore, the experiments are designed to capture more than 10 samples per period, much more than the theoretical minimum according to the sampling theorem³⁷ as it is applied to a Fourier limited pulse in space and time. The overall delay is ~ 130 fs, which is sufficient to scan the overlap of the 10 fs pulses and provide a spectral resolution of about 13 nm over the bandwidth of interest after the Fourier transform (FFT). That is about 16 wavelength points in the region between 700 and 900 nm. The resolution can be further enhanced with a longer delay line.

The above procedure along with the TERMITES algorithm produces a reference (known) linearly polarized pulse. A simple interference of this reference pulse with an unknown more complex structured pulse, like a CVP, is sufficient to reveal the full spatial and temporal structure of the latter. Such an experimental setup is given in Fig. 2(b). After the first beam splitter [BS1 in Fig. 2(b)], two replicas of the pulse are created that travel in two separate arms of a Mach-Zehnder interferometer. The right part of the interferometer carries the reference pulse, while the left arm is used to generate a CVP, which then propagates to the final beam splitter [BS2 in Fig. 2(b)] where the two pulses recombine and the interference takes place. In this case, the beam splitter has to be polarization independent, as the polarization of the unknown pulse is spatially dependent. An interference image at -6.5 fs delay between the linearly polarized pulse and the CVP is shown in the inset of Fig. 2(b). The interference pattern is antisymmetric with respect to the center of the radially polarized pulse, which is a manifestation of the radial polarization shown with yellow arrows. A small difference in the curvature between the two pulses manifests as shorter (longer) fringes at the (center) edge.

To ensure that dispersion in both paths of the Mach-Zehnder interferometer is equal to that of the TERMITES experiment, we introduce dispersive glasses DG1 and DG2 [see Fig. 2(b)]. As an example, here, we characterize a radially polarized pulse that is generated from a segmented waveplate.^{17,38,39} Our polarization transformer consists of eight achromatic half-wave plates with the relative orientation of the fast axis at $\pm 11^\circ$, $\pm 34^\circ$, $\pm 56^\circ$, and $\pm 79^\circ$. The joints between the waveplates scatter part of the incident light, which is removed by a $75\ \mu\text{m}$ pinhole placed at the Fourier plane. An iris placed before the focusing mirror is used to select the size of the radially polarized pulse that has to be smaller or equal to the reference. Any diffraction introduced by the iris will also be filtered out by the pinhole. The $75\ \mu\text{m}$ pinhole allows us to remove diffracted light from the segmented waveplate without affecting the cylindrical vector nature of the pulse.

A half-waveplate is placed before the segmented waveplate to rotate the input polarization and hence select the output polarization that can be either radial or azimuthal.

The filtered pulse travels to a delay line that creates a variable delay between the CVP and the reference pulse. The Thorlabs TSGNF5 single axis piezoelectric stage along with a hollow retroreflector was used for the delay line. The interferogram is then captured by the camera. A polarizer before the camera is used not only for increasing the signal to noise ratio but also to characterize the two orthogonal polarizations of the CVP. The latter is achieved by rotating the polarizer at $\pm 45^\circ$ with respect to the polarization of the reference pulse. Hence, two measurements are required. The delay between the polarizations is assumed to be zero because of the working principle of the achromatic segmented waveplate. Indeed, the group delay between the waves traveling along the fast and slow axes of each segment of our waveplate is considered identical (within the manufacturing tolerance of $\lambda/40$), and therefore, the two orthogonal polarizations are not separated along the propagation direction. In case that the relative phase is not known, it can be retrieved with a third measurement by rotating the polarization of the reference pulse by 45° with a half-waveplate at 22.5° . Another approach would be to use a reference pulse polarized at 45° and interfere it with the x and y components of the unknown pulse on a polarizing beam splitter while simultaneously recording the interference pattern on two image sensors on a single pass of the linear stage. This method is similar to POLLIWOG.⁴⁰

B. Analysis of the recorded data

In this section, we briefly discuss the TERMITES algorithm and we present the extra analysis steps needed for the characterization of CVPs. The TERMITES method is used for the spatiotemporal characterization of linearly polarized pulses up to a constant spectral phase corresponding to the carrier envelope phase. Our approach inherits these limitations.

In TERMITES, a pulse is interfered with a magnified replica of itself. A delay line is used to scan the unknown pulse with the reference. The interference pattern is then recorded by a digital camera, and an image for each relative delay is stored in a computer, resulting in a 3D dataset [see Fig. 3(a)]. For each pixel across all images, an interferogram is captured, which is the collected energy during the exposure period transferred to the sensor by the two pulses, as a function of the delay. This signal is proportional to the time integral of the intensity of the total electric field and can be written as

$$\begin{aligned} S(\mathbf{r}, \tau) &= \int |E_R(\mathbf{r}, t) + E(\mathbf{r}, t - \tau)|^2 dt \\ &= I(\mathbf{r}) + I_R(\mathbf{r}) + \int [E_R(\mathbf{r}, t)E^*(\mathbf{r}, t - \tau) \\ &\quad + E_R^*(\mathbf{r}, t)E(\mathbf{r}, t - \tau)] dt, \end{aligned} \quad (1)$$

with the subscript “R” denoting the reference (diverging) pulse and τ denoting the delay. The signal on a central pixel is shown in Fig. 3(b). A constant signal is observed when there is no overlap of the pulses, mathematically described by the first two terms of Eq. (1), and an interference signal when they overlap, mathematically described by the integral. The term $s(\mathbf{r}, \tau) = \int E_R(\mathbf{r}, t)E^*(\mathbf{r}, t - \tau)dt$ is the cross

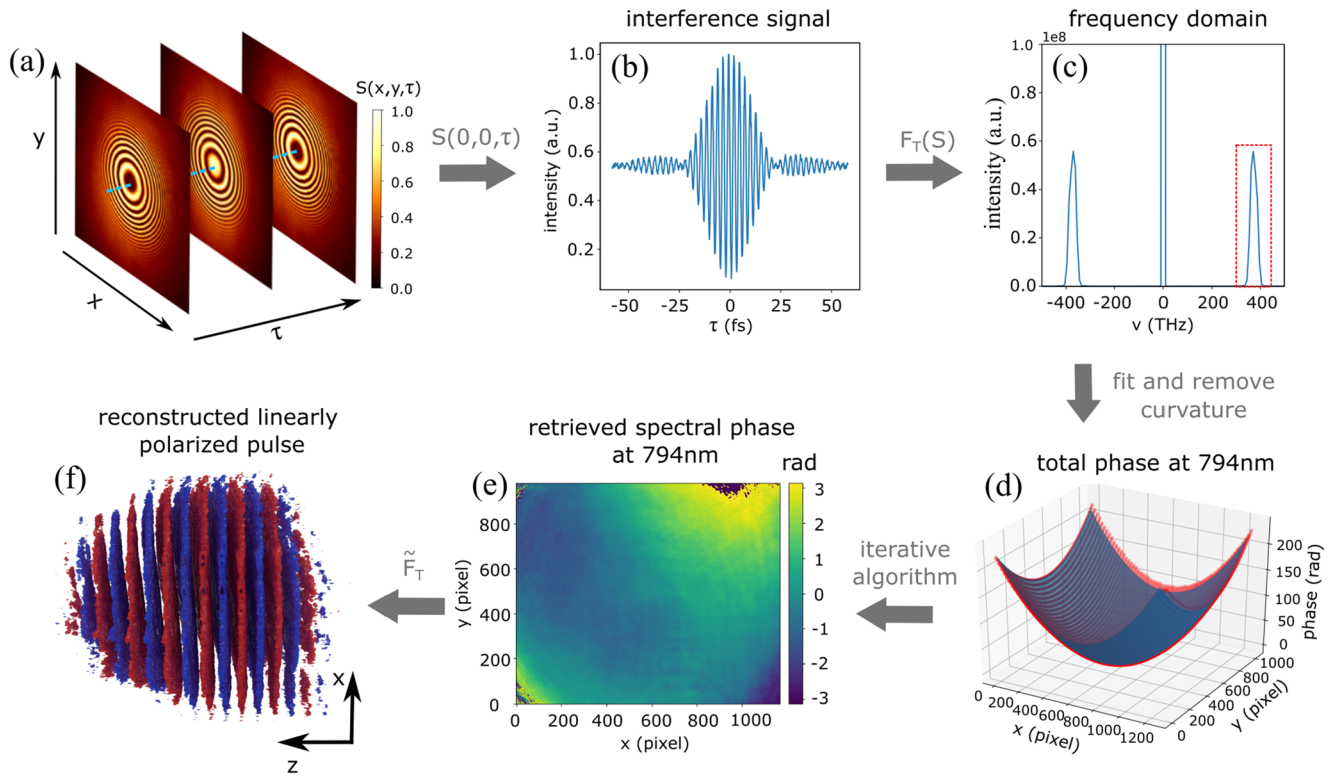


FIG. 3. A schematic description of image processing in the TERMITES algorithm. The data are acquired from the setup described in Fig. 2(a). (a) A sequence of interference images captured by a digital camera for successive delays τ of the reference pulse. (b) The cross-correlation signal, $S(x, y, \tau)$, at a single pixel of the camera sensor. That is the measured intensity as a function of the delay. (c) The spectrum derived by a fast Fourier transform (F_T) performed on the cross-correlation signal of the pixel. (d) Unwrapped phase data (red dots) and the quadratic fitted surface (blue) close to the central wavelength (≈ 800 nm). The fitted phase is removed from the total spatially depended phase to reveal the phase due to the STC. (e) The retrieved phase at 794 nm after the application of the iterative algorithm. (f) The 3D reconstruction of the pulse in time and space through an inverse Fourier transform (\hat{F}_T^{-1}) of the retrieved amplitude and phase data.

correlation of the two fields. Hence, Eq. (1) takes the form

$$S(\mathbf{r}, \tau) = I(\mathbf{r}) + I_R(\mathbf{r}) + s(\mathbf{r}, \tau) + s^*(\mathbf{r}, \tau). \quad (2)$$

A Fourier transform is then performed for every pixel. The frequency domain signal is now described by the equation

$$S(\mathbf{r}, \omega) = F_T[S(\mathbf{r}, \tau)] = F_T[I(\mathbf{r}) + I_R(\mathbf{r})] + s(\mathbf{r}, \omega) + s^*(\mathbf{r}, -\omega), \quad (3)$$

with F_T denoting the time to frequency Fourier transform operator. The equation describes the presence of a zero frequency term, derived from the Fourier transform of the time stationary term, and two frequency signals with equal amplitude and at symmetric frequencies. Figure 3(c) shows the results derived from the above analysis at a position in the central part of the pulse. A zero frequency term and two symmetric peaks with central wavelength at around 800 nm, in accordance with the central wavelength of our laser, are formed by the Fourier transform.

The result of the above procedure leads to two sets of images. One carries the intensity distribution at each frequency and the other carries the spectral phase. The negative frequencies can be derived by the complex conjugate of the positive and hence are redundant for the analysis. Additionally, the noise free spectral range is

~ 700 to 900 nm. Thus, only images at wavelengths within the bandwidth of the laser are needed for the analysis, and hence, the processing time is reduced significantly without any loss of information.

The Fourier transform of the cross correlation of two signals, $E(\mathbf{r}, t)$ and $E_R(\mathbf{r}, t)$, is equal to the product of their spectra with one of them being complex conjugate, as in the cross-correlation integrand. In our case, we have $s(\mathbf{r}, \omega) = E_R(\mathbf{r}, \omega)E^*(\mathbf{r}, \omega)$. The amplitude and phase of the signal that we are interested are thus given by

$$|s(\mathbf{r}, \omega)| = A_R(\mathbf{r}, \omega)A(\mathbf{r}, \omega), \quad (4)$$

$$\arg(s(\mathbf{r}, \omega)) = \varphi_R(\mathbf{r}, \omega) - \varphi(\mathbf{r}, \omega), \quad (5)$$

with A being the amplitude of the spectrum and φ being the spectral phase.

In the TERMITES algorithm, the spectral phase that is created from the convex mirror is removed by fitting a quadratic surface to the phase data [Fig. 3(d)] and then an iterative algorithm is applied [Fig. 3(e)] until the retrieved spectral phase correctly reproduces the known relationship between the pulse and its expanded replica.¹⁴ An

inverse Fourier transform then reconstructs the linearly polarized pulse in time and space [Fig. 3(f)].

Following the characterization of the reference pulse, the Mach-Zehnder experiment is performed. A delay line is used to

scan the unknown CVP pulse with the characterized reference, and the interference pattern is again recorded on an image sensor; see Fig. 4(a). The total length of the delay line is $20\ \mu\text{m}$ and is scanned with a step of $20\ \text{nm}$, resulting in a total delay of $40\ \mu\text{m}$ and step

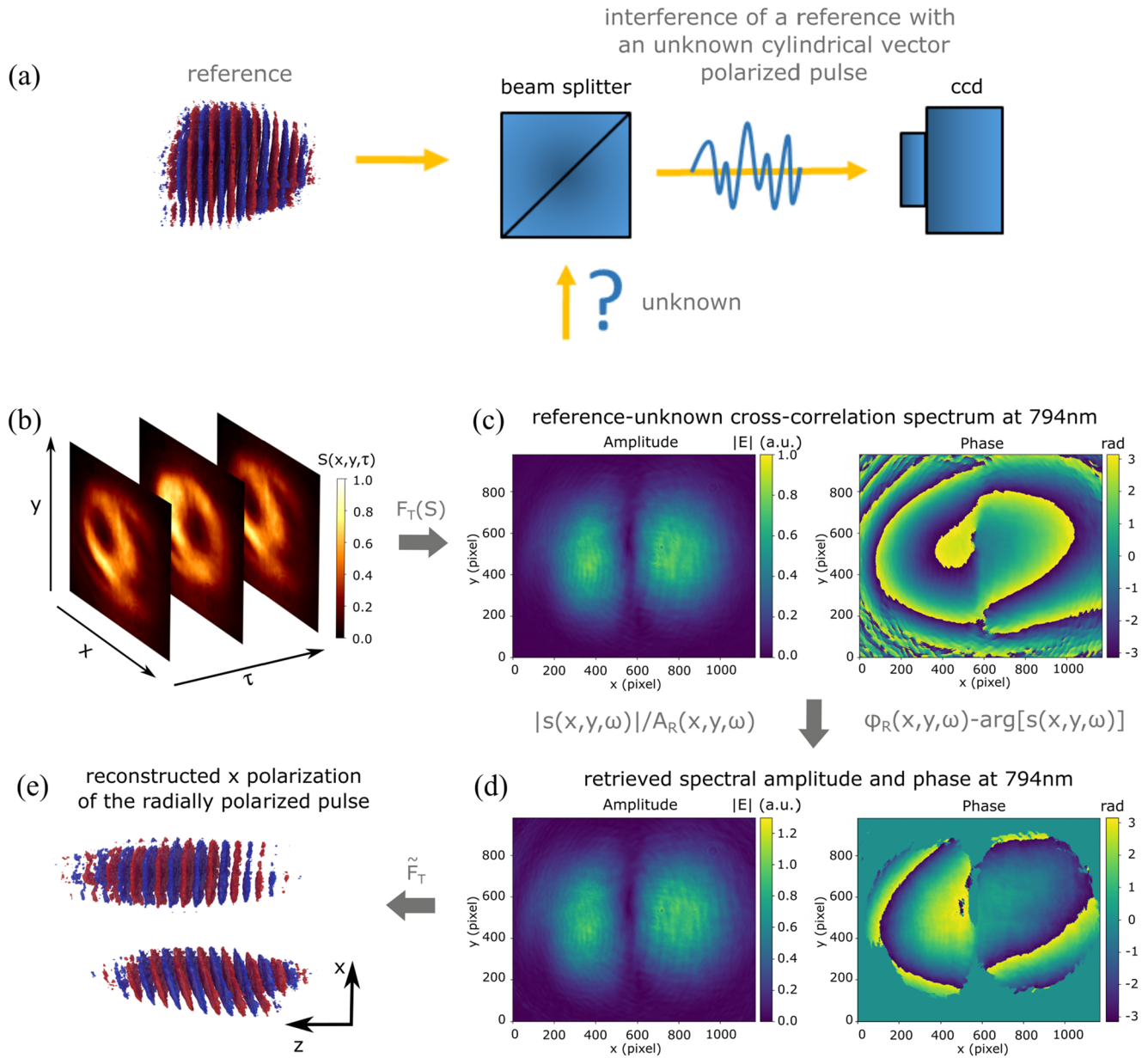


FIG. 4. TERMITES-MAZE method for the characterization of a radially polarized pulse. (a) A simplified schematic of the experiment, where the reference pulse from the previous part of the method is interfered with the unknown CVP. (b) A sequence of interference images captured by a digital camera for successive delays of the reference pulse with respect to the CVP. (c) Spectral amplitude and phase of the Fourier transformed interference images at $\lambda = 794\text{ nm}$. (d) The retrieved amplitude and phase of the x polarization of the radially polarized pulse at 794 nm after the division and subtraction of the reference pulse's amplitude and phase from the cross-correlation spectra. The spectral phase of the regions with field amplitude lower than 10% of the maximum has been masked to 0 phase value. We note that the form of the cross-correlation amplitude and phase maps [panel (c)] of the CVP and the reference linearly polarized pulse is mainly controlled by the field structure of the CVP [panel (d)]. (e) The 3D reconstruction of the x polarized component of the radially polarized pulse in space and time [where we assume $(z \sim ct)$].

of 40 nm for the two-way trip of the pulse. The captured data, consisting of 1000 interference patterns, are again transferred to the frequency domain, Figs. 4(b) and 4(c), where the amplitude and phase of the signal are given by Eqs. (4) and (5). However, in this case, the reference spectral amplitude and spectral phase are known, since they correspond to the characterized linearly polarized pulse. Therefore, the spectral amplitude and phase of the CVP are retrieved by a division of the spectral amplitudes and a subtraction of the spectral phases,

$$A(\mathbf{r}, \omega) = |s(\mathbf{r}, \omega)| / A_R(\mathbf{r}, \omega), \quad (6)$$

$$\varphi(\mathbf{r}, \omega) = \varphi_R(\mathbf{r}, \omega) - \arg(s(\mathbf{r}, \omega)). \quad (7)$$

The output is the frequency domain representation of the unknown CVP [Fig. 4(d)]. An inverse Fourier transform transfers the pulse to the time domain where the three dimensional shape of the pulse is reconstructed [Fig. 4(e)]. The procedure is then repeated for the orthogonal polarization, and the results are combined.

Figure 5 shows the spectral amplitude and spectral phase of the x and y polarizations of a radially polarized pulse at 794 nm as derived by the analysis. The spectral phase is calculated only on regions with field amplitude higher than 10% of the maximum of

the central wavelength. In these areas, the pulse has a phase difference of π between its left and right (or top-bottom) parts as expected for a CVP due to the polarization singularity in its center. The small deviation of the phase profile from the cylindrical symmetry is due to the existence of relatively weak space-time couplings, such as pulse front tilt and curvature, as can be seen in Fig. 6. The spectral amplitude and phase plots of the remaining wavelengths can be found in the supplementary as animations for both polarizations.

An inverse Fourier transform is applied to reconstruct the three dimensional shape of the pulse in the time domain. Figures 6(a)–6(d) show the $x-t$ and $y-t$ cross sections for the x and y polarization, respectively, of a radially polarized pulse and their 3D reconstruction as an isosurface at half of the maximum amplitude. The pulse is 10 fs long, and it is clear that apart from a small curvature and a small pulse front tilt in the x direction, it does not have significant aberrations. A similar small curvature and PFT also exist in the initial linearly polarized pulse, which is attributed to minor imperfections in the initial part of the setup.

In contrast, Fig. 7 shows the reconstruction of a pulse exhibiting PFT in its x direction. This is the initial pulse from the laser, and it has a PFT and an uneven distribution of intensity [see Figs. 7(a) and 7(b)] that it is corrected with a wedge [Figs. 6(a) and 6(b)]. The existence of the PFT offers an opportunity to apply the

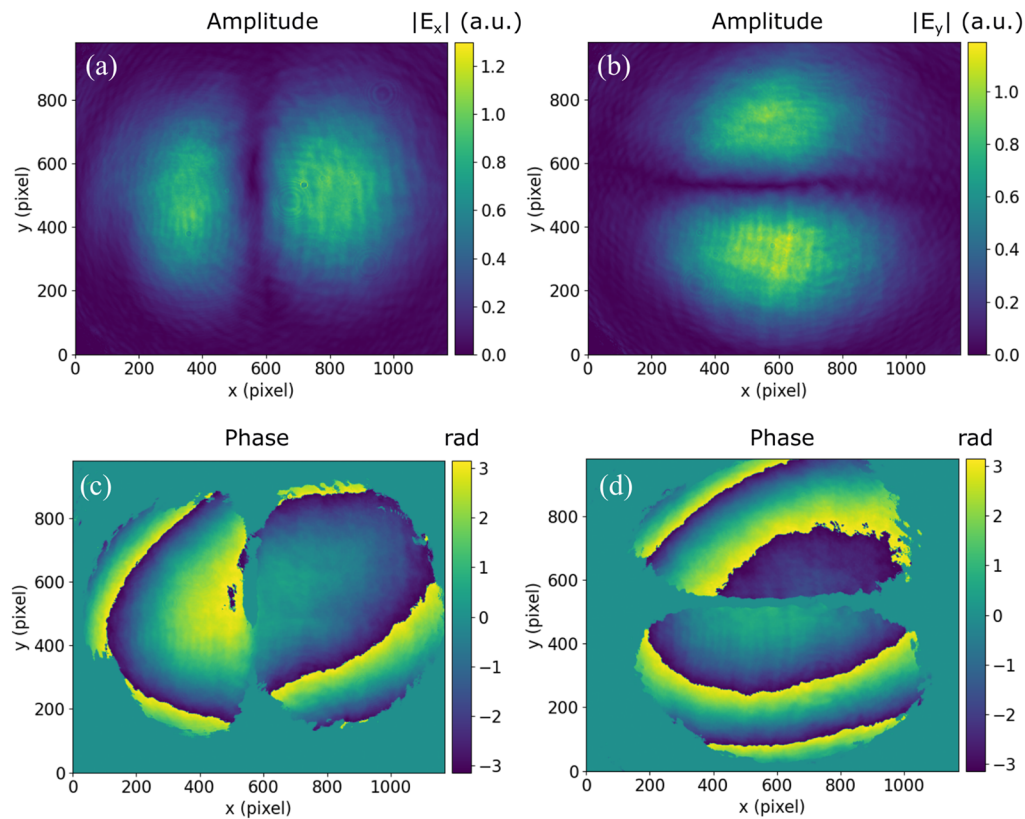


FIG. 5. Retrieved amplitude [(a) and (b)] and phase [(c) and (d)] of the horizontal [(a) and (c)] and vertical [(b) and (d)] polarizations of a radially polarized pulse at 794 nm according to the TERMITES-MAZE algorithm. The spectral phase in (c) and (d) exhibits a π phase difference between the left-right and top-bottom areas, respectively.

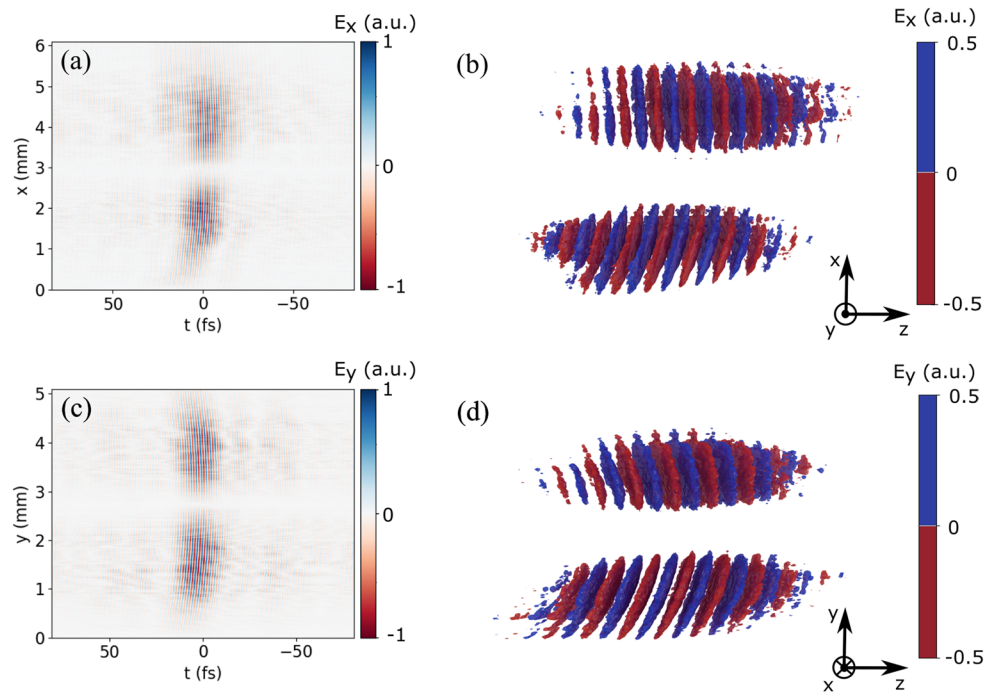


FIG. 6. (a) and (b) $x - t$ cross section of the x polarized electric field of a 10 fs radially polarized pulse and its isosurface plot at half of the maximum electric field value as it is reconstructed with the TERMITES-MAZE method. (c) and (d) $y - t$ cross section of the y polarized electric field of the same pulse and its isosurface plot.

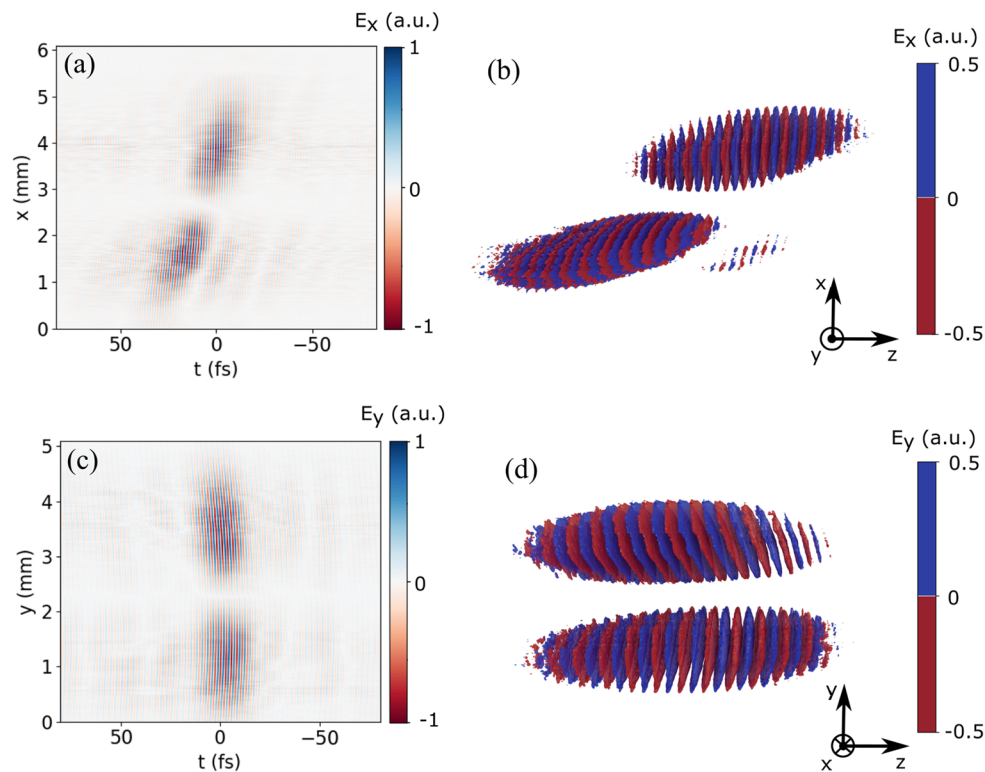


FIG. 7. (a) and (b) $x - t$ cross section of the x polarized electric field of a 10 fs radially polarized pulse exhibiting a PFT and its isosurface plot at half of the maximum electric field value as is reconstructed with the TERMITES-MAZE method. (c) and (d) $y - t$ cross section of the y polarized electric field of the same pulse and its isosurface plot.

developed method for the characterization and correction of the latter. The measured PFT is found to be about seven fs/mm, and it was retrieved by fitting a paraboloid to the spatially depended delay of the pulse, which is directly related to the spatially depended spectral phase provided by the analysis.⁴¹ A way to quickly correct the tilt is to insert a wedge. The induced PFT due to a wedge can be calculated from the following equation:⁵

$$\xi = \frac{\lambda_0 \tan(\theta)}{c} \frac{dn}{d\lambda}, \quad (8)$$

with λ_0 being the central wavelength of the pulse, c being the speed of light, n being the refractive index, and θ being the angle of the wedge. Here, we have used a commercially available 5° fused silica wedge plate in the path of the pulse. From Eq. (8), we calculate the PFT introduced by the wedge to be about 6 fs/mm. The wedge was inserted in such a way that influenced and corrected the profile of the pulse along the horizontal axis, x direction. The corrected pulse is shown in Fig. 6 and exhibits a PFT of about 0.5 fs/mm, which is close to the expected value from Eq. (8). The fact that the existence of the PFT on the generated CVP was discovered only during the development of the method highlights its practicality to any field employing such pulses.

III. CONCLUSIONS

In this paper, we have presented a technique for the spatiotemporal characterization of CVPs and we demonstrated its capabilities by a complete spatiotemporal characterization of a 10 fs radially polarized pulse. The technique is a Mach–Zehnder interferometry extension to the TERMITES method that allows us to overcome the limitation of the latter and to characterize pulses with polarization singularities. A radially polarized pulse exhibiting pulse front tilt was also characterized to illustrate the capabilities of the method.

In the current implementation, the method characterizes CVPs whose relative phase between the two orthogonal polarizations is *a priori* known, and hence, it is not measured. However, in certain cases, this relative phase is not known, for example, in pulses with dynamic polarization like polarization gates that are used for the generation of isolated attosecond pulses.⁴² The TERMITES-MAZE method can be easily extended for the characterization of such pulses by altering the setup to use a reference pulse polarized at 45° and interfere it with the x and y components of the unknown pulse on a polarizing beam splitter, similar to the POLLIWOG method.⁴⁰

Apart from the characterization of CVPs, the method can be applied to ultrashort light structures possessing a number of polarization or phase singularities. The latter is of paramount importance to transfer the field of topological optics⁴³ from monochromatic beams to singular pulses.⁴⁴ Additionally, many applications of CVPs such as free space communications or micro-machining can directly benefit from the method acting as a diagnostic tool that allows us to achieve an optimal pulse shape. Finally, TERMITES-MAZE can be employed to explore the generation, propagation, and applications of novel structured ultrafast pulses.

SUPPLEMENTARY MATERIAL

Supplementary material videos, *cvp_x.mp4* and *cvp_y.mp4*, present the spectral amplitude (left) and phase (right) plots of

the CVP pulse for each polarization, as they are retrieved by the TERMITES-MAZE method. Each frame in the videos corresponds to amplitude and phase plots at a single wavelength in the range 670–900 nm. The units in the horizontal and vertical axes are in pixels, with each pixel being 5.2 μm in size.

ACKNOWLEDGMENTS

The authors acknowledge support from the MOE Singapore (Grant No. MOE2016-T3-1-006), the UK's Engineering and Physical Sciences Research Council (Grant No. EP/M009122/1), the European Research Council (Advanced Grant No. FLEET-786851), and the Defense Advanced Research Projects Agency (DARPA) under the Nascent Light Matter Interactions program.

AUTHOR DECLARATIONS

Conflict of Interest

The authors declare no conflicts of interest.

DATA AVAILABILITY

The data that support the findings of this study are openly available in University of Southampton ePrints research repository at <https://doi.org/10.5258/SOTON/D1996>. A software package for the analysis of the experimental data has been developed in the Python programming language and can also be obtained from the University of Southampton ePrints research repository under the BSD three-clause license.²⁷

APPENDIX: CYLINDRICAL VECTOR PULSES

Cylindrical vector beams are solutions to Maxwell's equation whose amplitude, phase, and polarization are axially symmetric. They have been extensively studied, and they are routinely generated and characterized.⁴⁵ Their unique properties have found numerous applications, such as tight focusing,³⁸ efficient particle trapping,^{46,47} super-resolution microscopy,⁴⁸ dense optical 3D data storage,⁴⁹ and data encoding for optical communications,⁵⁰ to name a few. Furthermore, their space-polarization non-separability has been applied to extend the concepts and tools of quantum physics to “classically entangled” states.^{51,52}

Cylindrical vector pulses are the pulsed version of the cylindrical vector beams. Although they offer more opportunities for applications, they are less studied due to the difficulty of their generation and characterization. They share all of the characteristics that make these propagating light structures interesting with additional important features arising due to their pulsed nature. Their short duration renders them ideal for microprocessing of materials since they combine reduced thermal damage to the material with the increased efficiency and homogeneity of the radial polarization when used in micro-drilling.⁵³ In fact, single-cycle CVPs, termed “flying donuts,” exist,⁵⁴ for which applications in particle acceleration have been suggested. Moreover, such pulses exhibit topological structure with a number of localized singularities,⁴⁴ while their toroidal topology is ideal for engaging toroidal and anapole modes in matter.^{55,56}

REFERENCES

- ¹S. Akturk, X. Gu, P. Bowlan, and R. Trebino, "Spatio-temporal couplings in ultrashort laser pulses," *J. Opt.* **12**, 093001 (2010).
- ²G. Pretzler, A. Kasper, and K. J. Witte, "Angular chirp and tilted light pulses in CPA lasers," *Appl. Phys. B: Lasers Opt.* **70**, 1–9 (2000).
- ³H. Vincenti and F. Quéré, "Attosecond lighthouses: How to use spatiotemporally coupled light fields to generate isolated attosecond pulses," *Phys. Rev. Lett.* **108**, 113904 (2012).
- ⁴D. H. Froula, D. Turnbull, A. S. Davies, T. J. Kessler, D. Haberberger, J. P. Palastro, S.-W. Bahk, I. A. Begishev, R. Boni, S. Bucht *et al.*, "Spatiotemporal control of laser intensity," *Nat. Photonics* **12**, 262 (2018).
- ⁵A. Sainte-Marie, O. Gobert, and F. Quéré, "Controlling the velocity of ultrashort light pulses in vacuum through spatio-temporal couplings," *Optica* **4**, 1298–1304 (2017).
- ⁶C. Dorrer, "Spatiotemporal metrology of broadband optical pulses," *IEEE J. Sel. Top. Quantum Electron.* **25**, 1–16 (2019).
- ⁷P. Bowlan, P. Gabolde, A. Shreenath, K. McGresham, R. Trebino, and S. Akturk, "Crossed-beam spectral interferometry: A simple, high-spectral-resolution method for completely characterizing complex ultrashort pulses in real time," *Opt. Express* **14**, 11892–11900 (2006).
- ⁸S. L. Cousin, J. M. Bueno, N. Forget, D. R. Austin, and J. Biegert, "Three-dimensional spatiotemporal pulse characterization with an acousto-optic pulse shaper and a Hartmann–Shack wavefront sensor," *Opt. Lett.* **37**, 3291–3293 (2012).
- ⁹E. M. Kosik, A. S. Radunsky, I. A. Walmsley, and C. Dorrer, "Interferometric technique for measuring broadband ultrashort pulses at the sampling limit," *Opt. Lett.* **30**, 326–328 (2005).
- ¹⁰A. S. Wyatt, I. A. Walmsley, G. Stibenz, and G. Steinmeyer, "Sub-10 fs pulse characterization using spatially encoded arrangement for spectral phase interferometry for direct electric field reconstruction," *Opt. Lett.* **31**, 1914–1916 (2006).
- ¹¹C. Dorrer, E. Kosik, and I. Walmsley, "Space-time characterization of ultrashort optical pulses using 2-dimensional shearing interferometry," in *Technical Digest. Summaries of Papers Presented at the Conference on Lasers and Electro-Optics. Postconference Technical Digest Cat. No. 01CH37170* (IEEE, 2001), pp. 78–79.
- ¹²P. Gabolde and R. Trebino, "Single-shot measurement of the full spatio-temporal field of ultrashort pulses with multi-spectral digital holography," *Opt. Express* **14**, 11460–11467 (2006).
- ¹³M. Miranda, M. Kotur, P. Rudawski, C. Guo, A. Harth, A. L'Huillier, and C. L. Arnold, "Spatiotemporal characterization of ultrashort laser pulses using spatially resolved Fourier transform spectrometry," *Opt. Lett.* **39**, 5142–5145 (2014).
- ¹⁴G. Pariente, V. Gallet, A. Borot, O. Gobert, and F. Quéré, "Space-time characterization of ultra-intense femtosecond laser beams," *Nat. Photonics* **10**, 547 (2016).
- ¹⁵K. J. Moh, X.-C. Yuan, J. Bu, D. K. Y. Low, and R. E. Burge, "Direct noninterference cylindrical vector beam generation applied in the femtosecond regime," *Appl. Phys. Lett.* **89**, 251114 (2006).
- ¹⁶F. Kong, H. Larocque, E. Karimi, P. B. Corkum, and C. Zhang, "Generating few-cycle radially polarized pulses," *Optica* **6**, 160–164 (2019).
- ¹⁷S. Carbajo, E. Granados, D. Schimpf, A. Sell, K.-H. Hong, J. Moses, and F. X. Kärtner, "Efficient generation of ultra-intense few-cycle radially polarized laser pulses," *Opt. Lett.* **39**, 2487–2490 (2014).
- ¹⁸N. Papasimakis, T. Raybould, V. A. Fedotov, D. P. Tsai, I. Youngs, and N. I. Zheludev, "Pulse generation scheme for flying electromagnetic doughnuts," *Phys. Rev. B* **97**, 201409 (2018).
- ¹⁹R. Trebino and D. J. Kane, "Using phase retrieval to measure the intensity and phase of ultrashort pulses: Frequency-resolved optical gating," *J. Opt. Soc. Am. A* **10**, 1101–1111 (1993).
- ²⁰C. Iaconis and I. A. Walmsley, "Spectral phase interferometry for direct electric-field reconstruction of ultrashort optical pulses," *Opt. Lett.* **23**, 792–794 (1998).
- ²¹A. Zdagkas, N. Papasimakis, V. Savinov, and N. I. Zheludev, "Space-time non-separable pulses: Constructing isodiffracting donut pulses from plane waves and single-cycle pulses," *Phys. Rev. A* **102**, 063512 (2020).
- ²²D. Strickland and G. Mourou, "Compression of amplified chirped optical pulses," *Opt. Commun.* **55**, 447–449 (1985).
- ²³S. W. Jolly, "Focused fields of ultrashort radially polarized laser pulses having low-order spatiotemporal couplings," *Phys. Rev. A* **103**, 033512 (2021).
- ²⁴B. Alonso, I. Lopez-Quintas, W. Holgado, R. Drevinskas, P. G. Kazansky, C. Hernández-García, and Í. J. Sola, "Complete spatiotemporal and polarization characterization of ultrafast vector beams," *Commun. Phys.* **3**, 151 (2020).
- ²⁵R. Beer, *Remote Sensing by Fourier Transform Spectrometry* (John Wiley & Sons, 1992), Vol. 170.
- ²⁶C. W. Wells, A. E. Potter, and T. H. Morgan, "Near-infrared spectral imaging Michelson interferometer for astronomical applications," *Proc. SPIE* **0226**, 61–65 (1980).
- ²⁷A. Zdagkas, *Termites-maze Python Module* (University of Southampton, 2021).
- ²⁸L. Allen, M. W. Beijersbergen, R. J. C. Spreeuw, and J. P. Woerdman, "Orbital angular momentum of light and the transformation of Laguerre–Gaussian laser modes," *Phys. Rev. A* **45**, 8185–8189 (1992).
- ²⁹H. Rubinsztein-Dunlop, A. Forbes, M. V. Berry, M. R. Dennis, D. L. Andrews, M. Mansuripur, C. Denz, C. Alpmann, P. Banzer, T. Bauer, E. Karimi, L. Marrucci, M. Padgett, M. Ritsch-Marte, N. M. Litchinitser, N. P. Bigelow, C. Rosales-Guzmán, A. Belmonte, J. P. Torres, T. W. Neely, M. Baker, R. Gordon, A. B. Stilgoe, J. Romero, A. G. White, R. Fickler, A. E. Willner, G. Xie, B. McCorman, and A. M. Weiner, "Roadmap on structured light," *J. Opt.* **19**, 013001 (2016).
- ³⁰A. Zdagkas, Y. Shen, C. McDonnell, J. Deng, G. Li, T. Ellenbogen, N. Papasimakis, and N. I. Zheludev, "Observation of Toroidal Pulses of Light," *arXiv:2102.03636* [physics.optics] (2021).
- ³¹Y. Shen, Y. Hou, N. Papasimakis, and N. I. Zheludev, "Supertoroidal light pulses as electromagnetic skyrmions propagating in free space," *Nat. Comm.* **12**, 5891 (2021).
- ³²M. A. Porras, "Diffraction effects in few-cycle optical pulses," *Phys. Rev. E* **65**, 026606 (2002).
- ³³D. Hoff, M. Krüger, L. Maisenbacher, A. M. Saylor, G. G. Paulus, and P. Hommelhoff, "Tracing the phase of focused broadband laser pulses," *Nat. Phys.* **13**, 947 (2017).
- ³⁴Y. Zhang, D. Zille, D. Hoff, P. Wustelt, D. Würzler, M. Möller, A. M. Saylor, and G. G. Paulus, "Observing the importance of the phase-volume effect for few-cycle light-matter interactions," *Phys. Rev. Lett.* **124**, 133202 (2020).
- ³⁵A. Forbes, A. Aiello, and B. Ndagano, "Classically entangled light," in *Progress in Optics* (Elsevier, 2019), Vol. 64, pp. 99–153.
- ³⁶V. V. Lozovoy, I. Pastirk, and M. Dantus, "Multiphoton intrapulse interference. IV. Ultrashort laser pulse spectral phase characterization and compensation," *Opt. Lett.* **29**, 775–777 (2004).
- ³⁷C. E. Shannon, "Communication in the presence of noise," *Proc. IRE* **37**, 10–21 (1949).
- ³⁸R. Dorn, S. Quabis, and G. Leuchs, "Sharper focus for a radially polarized light beam," *Phys. Rev. Lett.* **91**, 233901 (2003).
- ³⁹G. Machavariani, Y. Lumer, I. Moshe, A. Meir, and S. Jackel, "Efficient extracavity generation of radially and azimuthally polarized beams," *Opt. Lett.* **32**, 1468–1470 (2007).
- ⁴⁰W. J. Walecki, D. N. Fittinghoff, A. L. Smirl, and R. Trebino, "Characterization of the polarization state of weak ultrashort coherent signals by dual-channel spectral interferometry," *Opt. Lett.* **22**, 81–83 (1997).
- ⁴¹S. W. Jolly, O. Gobert, and F. Quéré, "Spatio-temporal characterization of ultrashort laser beams: A tutorial," *J. Opt.* **22**, 103501 (2020).
- ⁴²I. J. Sola, E. Mével, L. Elouga, E. Constant, V. Strelkov, L. Poletto, P. Villoresi, E. Benedetti, J.-P. Caumes, S. Stagira *et al.*, "Controlling attosecond electron dynamics by phase-stabilized polarization gating," *Nat. Phys.* **2**, 319 (2006).
- ⁴³M. R. Dennis, K. O'Holleran, and M. J. Padgett, "Singular optics: Optical vortices and polarization singularities," in *Progress in Optics* (Elsevier, 2009), Chap. 5, Vol. 53, pp. 293–363.
- ⁴⁴A. Zdagkas, N. Papasimakis, V. Savinov, M. R. Dennis, and N. I. Zheludev, "Singularities in the flying electromagnetic doughnuts," *Nanophotonics* **8**, 1379–1385 (2019).
- ⁴⁵Q. Zhan, "Cylindrical vector beams: From mathematical concepts to applications," *Adv. Opt. Photonics* **1**, 1–57 (2009).

- ⁴⁶M. Michihata, T. Hayashi, and Y. Takaya, "Measurement of axial and transverse trapping stiffness of optical tweezers in air using a radially polarized beam," *Appl. Opt.* **48**, 6143–6151 (2009).
- ⁴⁷H. Moradi, V. Shahabadi, E. Madadi, E. Karimi, and F. Hajizadeh, "Efficient optical trapping with cylindrical vector beams," *Opt. Express* **27**, 7266–7276 (2019).
- ⁴⁸R. Chen, K. Agarwal, C. J. R. Sheppard, and X. Chen, "Imaging using cylindrical vector beams in a high-numerical-aperture microscopy system," *Opt. Lett.* **38**, 3111–3114 (2013).
- ⁴⁹X. Li, Y. Cao, and M. Gu, "Superresolution-focal-volume induced 3.0 Tbytes/disk capacity by focusing a radially polarized beam," *Opt. Lett.* **36**, 2510–2512 (2011).
- ⁵⁰G. Milione, T. A. Nguyen, J. Leach, D. A. Nolan, and R. R. Alfano, "Using the nonseparability of vector beams to encode information for optical communication," *Opt. Lett.* **40**, 4887–4890 (2015).
- ⁵¹T. Konrad and A. Forbes, "Quantum mechanics and classical light," *Contemp. Phys.* **60**, 1–22 (2019).
- ⁵²M. McLaren, T. Konrad, and A. Forbes, "Measuring the nonseparability of vector vortex beams," *Phys. Rev. A* **92**, 023833 (2015).
- ⁵³O. J. Allegre, W. Perrie, S. P. Edwardson, G. Dearden, and K. G. Watkins, "Laser microprocessing of steel with radially and azimuthally polarized femtosecond vortex pulses," *J. Opt.* **14**, 085601 (2012).
- ⁵⁴R. W. Hellwarth and P. Nouchi, "Focused one-cycle electromagnetic pulses," *Phys. Rev. E* **54**, 889–895 (1996).
- ⁵⁵T. Raybould, V. Fedotov, N. Papasimakis, I. Youngs, and N. Zheludev, "Focused electromagnetic doughnut pulses and their interaction with interfaces and nanostructures," *Opt. Express* **24**, 3150–3161 (2016).
- ⁵⁶T. Raybould, V. A. Fedotov, N. Papasimakis, I. Youngs, and N. I. Zheludev, "Exciting dynamic anapoles with electromagnetic doughnut pulses," *Appl. Phys. Lett.* **111**, 081104 (2017).